Noninvasive vascular ultrasound elastography applied to the characterization of experimental aneurysms and follow-up after endovascular repair

Jérémie Fromageau[1]**, Sophie Lerouge**[2,5]**, Roch Listz Maurice**[1,4,5]**, Gilles Soulez**[3,4,5] **and Guy Cloutier**[1,4,5]

[1] Laboratory of Biorheology and Medical Ultrasonics, University of Montreal Hospital Research Center (CRCHUM), Montréal, Québec, H2L 2W5, Canada
[2] Laboratory of Endovascular Biomaterials, University of Montreal Hospital Research Center (CRCHUM), Montréal, Québec, H2L 2W5, Canada; and Department of Mechanical Engineering, École de Technologie Supérieure, Montréal, Québec, H3C 1K3, Canada
[3] Department of Radiology, University of Montreal Hospital, Montréal, Québec, H2L 4M1, Canada
[4] Department of Radiology, Radio-Oncology and Nuclear Medicine, University of Montreal, Montréal, Québec, H3C 3J7, Canada
[5] Institute of Biomedical Engineering, University of Montreal, Montréal, Québec, H3T 1J4, Canada

E-mail: guy.cloutier@umontreal.ca

Abstract
Experimental and simulation studies were conducted to noninvasively characterize abdominal aneurysms with ultrasound (US) elastography before and after endovascular treatment. Twenty three dogs having bilateral aneurysms surgically created on iliac arteries with venous patches were investigated. In a first set of experiments, the feasibility of elastography to differentiate vascular wall elastic properties between the aneurismal neck (healthy region) and the venous patch (pathological region) was evaluated on six dogs. Lower strain values were found in venous patches ($p < 0.001$). In a second set of experiments, 17 dogs having endovascular repair (EVAR) by stent graft (SG) insertion were examined three months after SG implantation. Angiography, color Doppler US, examination of macroscopic sections and US elastography were used. The value of elastography was validated with the following end points by considering a solid thrombus of a healed aneurysm as a structure with small deformations and a soft thrombus associated with endoleaks as a more deformable tissue: (1) the correlation between the size of healed organized thrombi estimated by elastography and by macroscopic examinations; (2) the correlation between the strain amplitude measured within vessel wall elastograms and the leak size; and (3) agreement on the presence and size of endoleaks as determined by elastography and by combined reference imaging modalities (angiography + Doppler US). Mean surfaces of solid thrombi

estimated with elastography were found correlated with those measured on macroscopic sections ($r = 0.88$, $p < 0.001$). Quantitative strain values measured within the vessel wall were poorly linked with the leak size ($r = 0.12$, $p = 0.5$). However, the qualitative evaluation of leak size in the aneurismal sac was very good, with a Kappa agreement coefficient of 0.79 between elastography and combined reference imaging modalities. In summary, complementing B-scan and color Doppler, noninvasive US elastography was found to be potentially a relevant tool for aneurismal follow-up after EVAR, provided it allows geometrical and mechanical characterizations of the solid thrombus within the aneurismal sac. This elasticity imaging technique might help detecting potential complications during follows-up subsequent to EVAR.

(Some figures in this article are in colour only in the electronic version)

1. Introduction

Abdominal aortic aneurysm (AAA) rupture is a major cause of mortality, responsible for more than 15 000 deaths each year in the USA (Hoyert *et al* 2006). An aneurysm ruptures when the wall of the distended artery fails to support stresses from internal blood flow, leading to a high risk of sudden death or severe disability. Nevertheless, the risk of rupture is small relative to the population of individuals with AAA. Because of a lack of reliable methods to predict aneurismal rupture, the choice whether to treat AAA is based on relative risk criteria such as aneurysm maximum diameter and growth rate. The loss of elasticity of the aortic wall is a known risk factor for rupture (Lasheras 2007). Consequently, vascular ultrasound (US) elastography, which is an imaging method that maps in color the strain within an arterial structure of interest, could contribute to improve management of this disease.

Open surgical repair of the aneurismal segment by a vascular prosthesis is currently the standard treatment for preventing aneurysm rupture. In comparison, endovascular aneurysm repair (EVAR) of AAA with a stent-graft (SG) offers a 3% reduction of peri-operative mortality (Greenhalgh 2004, Prinssen *et al* 2004). However, after 4 years, when compared with surgery, all-cause mortality is similar and more complications are observed in the EVAR group (EVAR trial participants 2005). Several drawbacks limit the long-term efficacy of EVAR (Thomas *et al* 2005, Seriki *et al* 2006, Hiramoto *et al* 2007). In particular endoleaks, defined as a persistent flow in the aneurismal sac, require a regular and lifelong follow-up to detect their occurrence.

Presence of endoleaks after EVAR increases the risk of aneurysm expansion (Uflacker and Robison 2001). Clinical follow-up presently includes computed tomography (CT) scan and US examinations. CT scan is the most reliable technique for detecting endoleaks but it requires contrast injection and exposure to ionizing radiation (Veith *et al* 2002). Growth or shrinkage of the aneurismal sac can be observed on B-scan US (Gorham *et al* 2004). More commonly, Doppler US is used to detect leaks inside the aneurismal sac, however it is less sensitive than CT (Sun 2006). Monitoring the pulse wall motion (PWM) was proposed to evaluate the aneurismal sac pressurization caused by a leak (Schurink *et al* 2000). PWM has been shown to be linked with the pulse pressure but not with the mean sac pressure. This limits the impact of this approach, since an aneurysm with a small PWM and high mean sac pressure can still expand. Recently, direct measurement of sac pressurization with an implantable wireless device was proposed (Chaer *et al* 2006). It is an attractive alternative as it correlates

well with invasive pressure measurements, but the method is itself invasive and also expensive. In addition, measurement variability due to pulsatility artifacts or sensor positioning within the thrombus instead of the leaky region of the sac may occur (Hinnen *et al* 2006, 2007). As proposed in the current study, the potential advantage of vascular US elastography as a complementary follow-up imaging technique would be its capacity to provide noninvasively information on wall mechanical properties (strain, elasticity) simultaneously with the extent of the solid thrombus within the aneurismal sac (absence of deformation).

Elasticity imaging was initially developed as a deep palpation tool to detect hard inclusions in soft media, typically for breast cancer (Cespedes *et al* 1993b). Whereas conventional elastography uses US images acquired at different load levels to assess tissue mechanical properties, another approach tracks tissue motions produced by shear waves (Parker *et al* 1990, Sandrin *et al* 1999, Nightingale *et al* 2002). With either standard compression elastography or shear-wave elasticity imaging, strain can be computed from displacements estimated with Doppler tissue tracking (Parker *et al* 1990), cross correlations (Ophir *et al* 1991), frequency shifts estimated by power spectral analysis (Konofagou *et al* 1999), or by direct assessment of the strain tensor with a Lagrangian estimator (Maurice and Bertrand 1999). Other strain estimation methods can also be found in the literature. In the current study, the Lagrangian estimator was chosen to compute vascular elastograms.

The demonstration of the feasibility of US elastography to map arterial wall deformations is more recent. It was combined with intravascular US imaging to evaluate strain in atherosclerotic coronary and carotid arteries (deformed by the natural blood pulsation when *in vivo* scans are considered) (de Korte *et al* 1998, Brusseau *et al* 2001, Schaar *et al* 2003, Maurice *et al* 2005a). More recently, it was proposed to noninvasively investigate mechanical properties of superficial vessels such as the carotid (Schmitt *et al* 2007, Ribbers *et al* 2007). In noninvasive vascular elastography (NIVE), US data are transcutaneously recorded and deformations produced by the natural vessel wall pulsation are tracked, as in endovascular elastography. In the current study, NIVE was applied to the problem of AAA. The first objective was to evaluate the potential of NIVE to detect expected deformation differences between surgically created aneurismal venous walls and healthy sections of iliac arteries in a dog model. The second objective was to evaluate elastography for follow-up applications after EVAR by correlating NIVE measurements with endoleak occurrences and to study thrombus evolution (size and diameter expansion) following EVAR.

2. Materials and methods

2.1. Description of the elastography algorithm

The method used to assess tissue strain is based on the optical flow implementation of the 2D Lagrangian estimator (Maurice *et al* 2005b). When a load is applied on a tissue, there is a relationship between two consecutive images, I_1 and I_2 within corresponding small region of interests (ROIs). Basically, the Lagrangian estimation consists in solving a nonlinear minimization problem to find the relationship allowing an optimal match between images $I_1(x, y)$ and $I_2^{\text{lag}}(x, y)$. Its implementation can mathematically be formulated as

$$\text{MIN} \| l_1(x, y) - I_2^{\text{lag}}(x, y) \|, \tag{1}$$

where $I_1(x, y)$ is a given ROI in a 'pre-load' radio-frequency (RF) US image and $I_2^{\text{lag}}(x, y)$ is the corresponding ROI in the 'post-load' RF image compensated for tissue motion. $I_2^{\text{lag}}(x, y)$ can be expressed as

$$I_2^{\text{lag}}(x, y) = I_1(x + \Delta_{xx}x + \Delta_{xy}y, y + \Delta_{yy}y + \Delta_{yx}x), \tag{2}$$

where (x, y) defines the image coordinate system, the four parameters in this equation being the lateral deformation Δ_{xx}, the axial deformation Δ_{yy}, and the two shear components Δ_{xy} and Δ_{yx} describing shear deformations. Axial strains within experimental aneurysms were computed as $\varepsilon_{yy} = \Delta_{yy}$. Each measurement window (ROI), on which equations (1) and (2) were applied, was set to 110×10 pixels (2.1×1.5 mm^2) axially and laterally, respectively. The ROI size was chosen after preliminary tests with the current aneurismal database. This size is a compromise between good resolution (capacity to detect small objects) and precision (low variance). To improve the signal-to-noise ratio (SNR) of NIVE images, they were post-processed with a 5×5 pixels iterative median filter also applied to reduce lateral discontinuities of elastograms.

2.2. Signal preprocessing

Most US images exhibited large amplitude contrasts because of the SG metallic structure. During the exploratory phase of this study, we observed that the size of the SG on elastographic images was artificially increased. Inspired by similar observations (Cespedes and Ophir 1993b) and with the aim of reducing elastography artifacts caused by hyper-echoic signals, a log compression of RF echoes was performed. The log compression was applied according to equation (3), which preserved the phase and changed only the signal amplitude (Pesavento *et al* 1999).

$$r_{\log}(t) = \log(1 + 10|r(t)|)\, e^{i\varphi(r(t))} \tag{3}$$

where $r(t)$ is the RF signal and $\varphi(r(t))$ is its phase.

2.3. Experimental AAA in dogs

The study was performed on 23 mongrel dogs weighing 20–25 kg. Protocols for animal experimentation were approved by the Animal Care Committee of the Centre Hospitalier de l'Université de Montréal, in accordance with the guidelines of the Canadian Council of Animal Care. Aneurysms were surgically constructed in the left and right common iliac arteries by opening longitudinally the arteries and by suturing a jugular vein patch of the same animal over the opening. In order to study type II endoleak in the second phase, implantation of a collateral vessel was also performed during the surgery according to a previously published model (Soulez *et al* 2007). In the first set of experiments (phase 1, 6 dogs), animals were investigated three months after aneurysm creation. The purpose was to measure vascular wall strain values in the venous patch and in the native artery at the vicinity of the proximal neck (above the surgically created aneurysm). In the second set of experiments (phase 2, 17 dogs), Jostent SGs (Jomed, Rangendingen, Germany; diameters of 4–9 mm, lengths of 48 mm) were implanted in both aneurysms after surgical creation. On both sides, endoleaks were intentionally produced. Type I endoleaks (leakage at graft attachment sites) were created by applying a plastic deformation to the SG in the proximal neck. Type II endoleaks (retrograde flow coming from collateral branches) were created by an appropriate SG placement, which led to retrograde flow from the collateral vessel connected to the aneurysm (Lerouge *et al* 2004). Figure 1 shows a schematic view of the different leaks created in this study. For each dog, one vessel side was favored to heal (i.e., to form a solid organized thrombus) either by mechanical endothelial ablation during surgery ($n = 5$) (Raymond *et al* 2002), by endothelial ablation and thrombin injection ($n = 6$), or by ethylcellulose injection into the sac ($n = 6$). The contralateral aneurysm served as a control, and all animals were observed for a period of three months.

At the end of the study, dogs were sacrificed and the aorta and iliac arteries were harvested 'en bloc' and fixed in buffered formalin. A cutting-grinding system (Exakt Gmbh, Norderstedt,
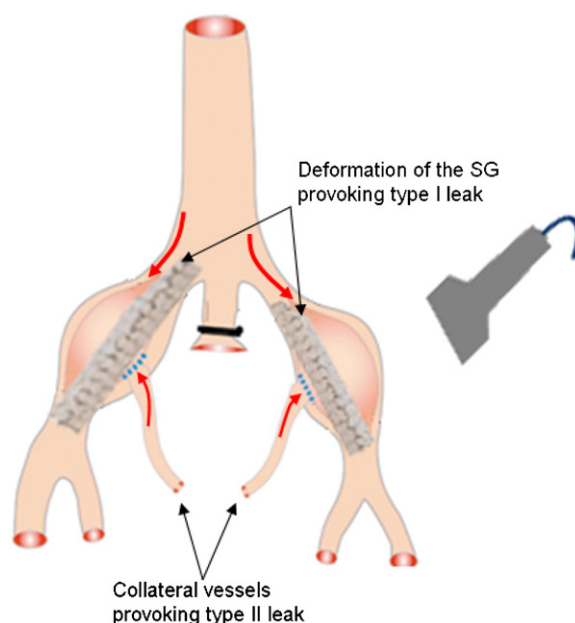
Figure 1. Schematic view of the animal model. The aneurysmal sac was created on both iliac arteries, and collateral vessels were connected to the sac to provoke type II leaks. During the stent graft (SG) placement, a plastic deformation of the SG in the proximal neck was created to mimic a type I leak.

Germany) was used to prepare macroscopic sections including the tissue/SG interface. The solid thrombus expanse inside of the aneurysm was estimated in three sections taken at the proximal, mid and distal portions of the sac.

2.3.1. Imaging (1st phase, no SG implantation). Imaging was conducted with a Sonix RP scanner (Ultrasonix, Vancouver, Canada) equipped with a 10 MHz linear array transducer with a 60% bandwidth. This US scanner provides a digitized RF signal sampled at 40 MHz that was used to compute elastograms. Depths of scanned arteries slightly changed with dogs and image sizes varied from 40 mm to 50 mm axially, and from 28 mm to 38 mm laterally. As a consequence, the frame rate ranged from 15 Hz to 19 Hz depending on the scanned animal. For the same reason, the focus depth varied from 25 mm to 35 mm. For each artery, longitudinal and axial cross sections were acquired noninvasively at the mid portion of the aneurysm and at the proximal neck. *Instantaneous* elastograms at these positions were calculated from two consecutive RF frames over the cardiac cycles available (3 to 5) in the data set (a positive strain in this study indicates tissue relaxation whereas a negative strain corresponds to a compression). *Instantaneous* elastograms were added to obtain *cumulated* strain images along the cardiac cycle. Quantitatively, the cumulated strain was calculated within ROI located in the venous patch and in the healthy portion of the artery proximally of the aneurismal neck. For both ROI, the maximum deformation corresponding to the cumulated strain from peak systole to end diastole was averaged over the total number of cycles available. These quantitative measurements provided a specific mechanical signature to each tissue structure.

2.3.2. Imaging (2nd phase, with SG implantation).　　RF ultrasound scans aimed to obtain elastograms were performed with the same Sonix RP scanner. For each artery, a complete longitudinal segment and three cross sections located at the proximal, mid and distal third of the aneurysm were scanned. In addition, a 10 MHz color Doppler examination followed on the same three cross-sectional locations of the artery with a Vivid 5 scanner (GE Vingmed, Horten, Norway). The registration between RF and color Doppler images was done by using the aneurysm limits as visual references. The precision of the registration was estimated at approximately $\pm$ 5 mm, thus the shape of the sac was expected to be similar on both types of images. A bilateral iliac angiography (Koordinat 3D II, Siemens Erlengen, Germany) was then performed through a femoral approach. Finally, the aneurysm expansion diameter was calculated on B-scan acquisitions by measuring the maximum diameter of the sac just before SG implantation and at sacrifice. Angiography, B-scans, color Doppler examinations and RF scans were done and reviewed simultaneously by a qualified vascular radiologist (G.S.). Elastography images were computed offline and analyzed by a blinded independent investigator (J.F.).

Detection and classification of endoleaks were based on the combined interpretation of angiography and color Doppler examinations. This combined method was also used to calculate the respective proportion of thrombosis and endoleak in the three cross sections considered for each aneurysm. Endoleak classification was achieved by averaging results obtained on the three cross sections. Endoleaks were thereafter arranged in three categories: 'large leaks' when the average percent of the vessel cross section occupied by the thrombus was less than 50%, 'small leaks' when the average percent was greater than 50% and 'absence of leak' when a complete sac thrombosis was observed.

With elastography, the criterion to diagnose an absence of leak was a homogeneous and constant in time strain in the sac, which means that no strain related to the cardiac pressure was observed because there was no open channels to convey the blood flow (which also included absence of strain within the artery wall). Absence of leak was also associated with small cumulated strain amplitudes ($<0.5\%$) leading to a 'poor' elastography image (dark image with no contrast), but providing by itself a useful information. On elastograms, there was visually a difference in terms of image rendering between high speed flow leaks and slow flow leaks. For slow flow leaks, the solid thrombus appeared as a homogeneous bloc with uniform strain, whereas the flow and the arterial wall gave two distinct homogeneous regions (the slow moving flow could produce correlated RF images and coherent elastograms). Slow flow leaks could be sorted as a small leak, if the region corresponding to the thrombus was more than 50% of the sac size, or as a large leak in the opposite case. For high speed flow leaks, due to RF decorrelated echoes, the flow in the sac appeared as a high variance region where both negative and positive strains were noted in the same area. High speed flow leaks were automatically classified as 'large leaks'. A mean solid thrombus area was estimated with elastography from the four scans of each artery and quantified in percentage of the whole sac surface. The mean surface of solid thrombi was also estimated on the three macroscopic sections by an independent operator for comparison.

Quantitative time-varying strain profiles were measured preferentially at the mid-portion of the venous patch (i.e., aneurysmal sac) selecting a region corresponding to the wall of the aneurysm. For each case, the maximum deformation between peak systole and end diastole was averaged over several cardiac cycles. To determine whether these strain values could also indicate an absence of leak, they were compared with the diagnosis classification done with combined color Doppler and angiography modalities.

Table 1. Cumulated strain in percent between peak systole and end diastole in the venous patch and in the arterial portion of the vessel wall. Statistics (mean ± standard deviation, two missing values) were computed by considering all pixels within the specified regions of interest (ROI) located in the venous patch and in the healthy artery for several cardiac cycles.

	Cumulated strain (%)					
	Dog 1	Dog 2	Dog 3	Dog 4	Dog 5	Dog 6
Left artery	8.4 ± 1.8	4.7 ± 1.2	×	4.0 ± 1.2	×	6.7 ± 1.7
Left vein	2.8 ± 1.0	2.3 ± 0.9	5.8 ± 1.2	2.5 ± 0.8	4.0 ± 0.3	2.9 ± 0.2
Right artery	7.4 ± 1.1	7.0 ± 1.8	6.4 ± 0.4	5.6 ± 0.6	4.1 ± 1.0	6.1 ± 1.2
Right vein	4.4 ± 0.2	4.0 ± 0.4	3.7 ± 0.7	2.6 ± 0.2	3.0 ± 0.3	2.5 ± 0.1

2.4. Statistical analyses

Quantitative variables are reported as mean ± standard deviation. If not otherwise specified, statistical analyses were made with the SigmaStat software (version 3.1, Systat Software, San Jose, CA). In phases 1 and 2, strains measured within the vessel wall and thrombus size were compared with Student pairwise t-tests. An analysis of variance (ANOVA) was performed to detect strain differences between animals. In phase 2 only, a weighted Kappa agreement test was used to evaluate inter-imaging modality agreements (Analyse it, Leeds, UK). A Pearson correlation coefficient was calculated to relate average percentages of thrombus, determined with elastography and macroscopic examinations.

3. Results

3.1. First phase, aneurysms without SG implantation three months after creation

Table 1 gives the mean range of cumulated strains (from peak systole to end diastole) for each dog and for each vessel side and type (venous patch or healthy artery). The missing values were due to the global decorrelation (over the whole image) of the two corresponding series, for which it was not possible to calculate reliable elastograms. The mean cumulated strain was significantly lower in the venous patch than in the healthy artery ($3.0 \pm 0.7\%$ versus $6.1 \pm 1.5\%$, $n = 10$, $p < 0.001$). In other words, the venous portion of the aneurysms was stiffer and less deformed by the cardiac pulsation. The mean cumulated strain also varied significantly from one dog to the other ($n = 6$, $p < 0.02$).

3.2. Second phase, aneurysms three months after creation and SG implantation

Twelve RF series among 136 were removed from the study because of the lack of correlation over the whole image between successive frames (technical success of 91%). Forty-four per cent of elastograms were sorted as 'large leaks', 35% as 'small leaks' and 21% were classified as no leak. Elastography estimated the mean size of thrombi at $59 \pm 36\%$ (0–100%). As shown in figure 2, elasticity images were particularly useful to bring information about the size of the solid thrombus within the sac. For the purpose of illustration, all image modalities considered in this study are displayed in this figure for dog 7 (first dog of the second phase).

The potential impact of elastography to the field of vascular imaging of aneurysms is further illustrated in figure 3. In panel (a), a small strain (amplitude $\leqslant 0.2\%$) is seen in the whole sac, suggesting that this aneurysm was completely filled with a solid thrombus
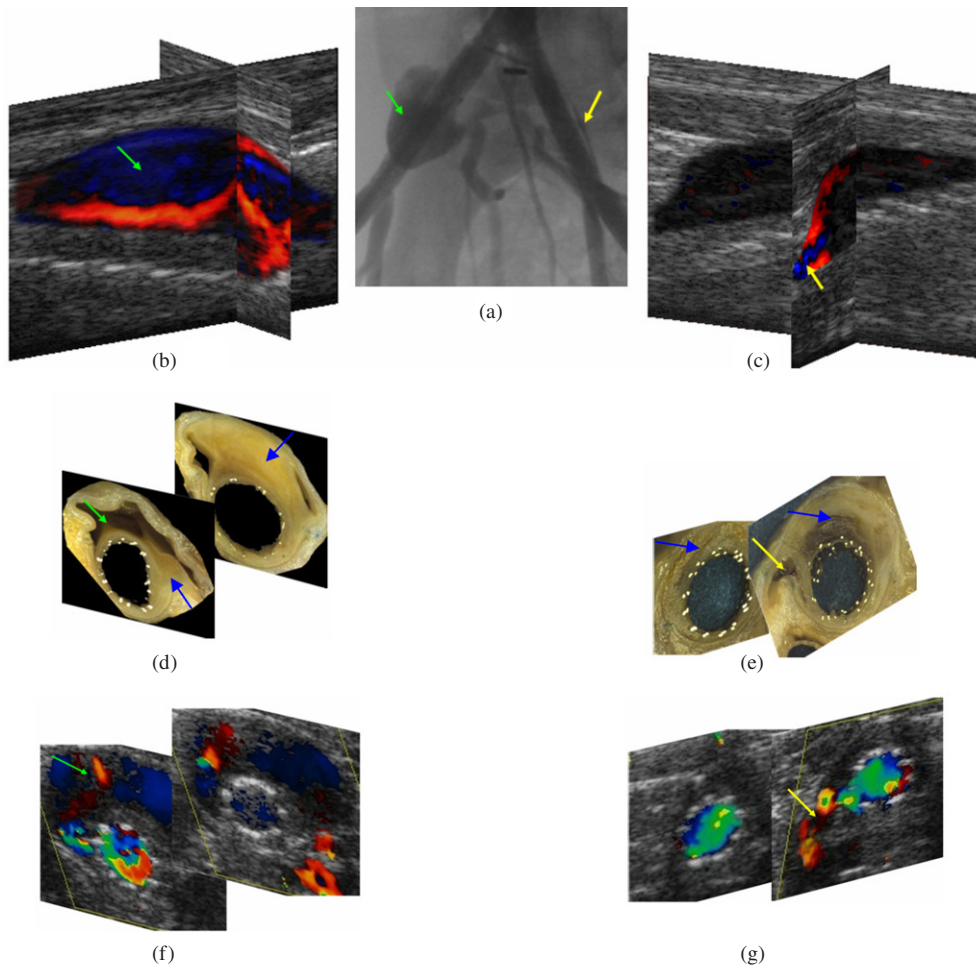
Figure 2. Set of images considered in this study (examples for dog #7). On each panel, green arrows indicate an important leak on the right iliac artery, whereas yellow arrows correspond to a small leak on the left artery. (a) X-ray angiogram with a large leak on the right aneurysm (left side of the image) and a small leak on the left. (b) Longitudinal and cross-sectional instantaneous elastograms (diastolic phase) of the right aneurysm, the arterial wall (strains in blue), the large leak (strains in black and blue) and a solid thrombus (strains in orange) are visible. Note that this corresponds to a slow flow leak, although the flow speed is small, the leak is defined as large because of the small proportion of solid thrombus. (c) Instantaneous elastograms of the left aneurysm that was almost filled with a solid thrombus as shown by the dark strains in most part of the sac. The small leak with strains in blue was detected on the mid cross-sectional elastogram. (d) and (e) are the corresponding macroscopic sections of the right and left arteries, respectively, where solid thrombi are shown with blue arrows. (f) and (g) are color-Doppler cross-sectional images.

without leak. In panel (b), the SG and thrombus deformed similarly and appeared on the elastogram as a homogeneous strain of approximately −1.5%, whereas the leak and arterial wall experienced positive strains of 0.5% and 1.5%, respectively. That case was classified as a small leak with a solid thrombus expanse of 50%. Strain values in the wall and in the solid thrombus are in opposite signs due to displacements in these two regions having opposite directions. This artifact is probably due to the configuration of the artery where two soft
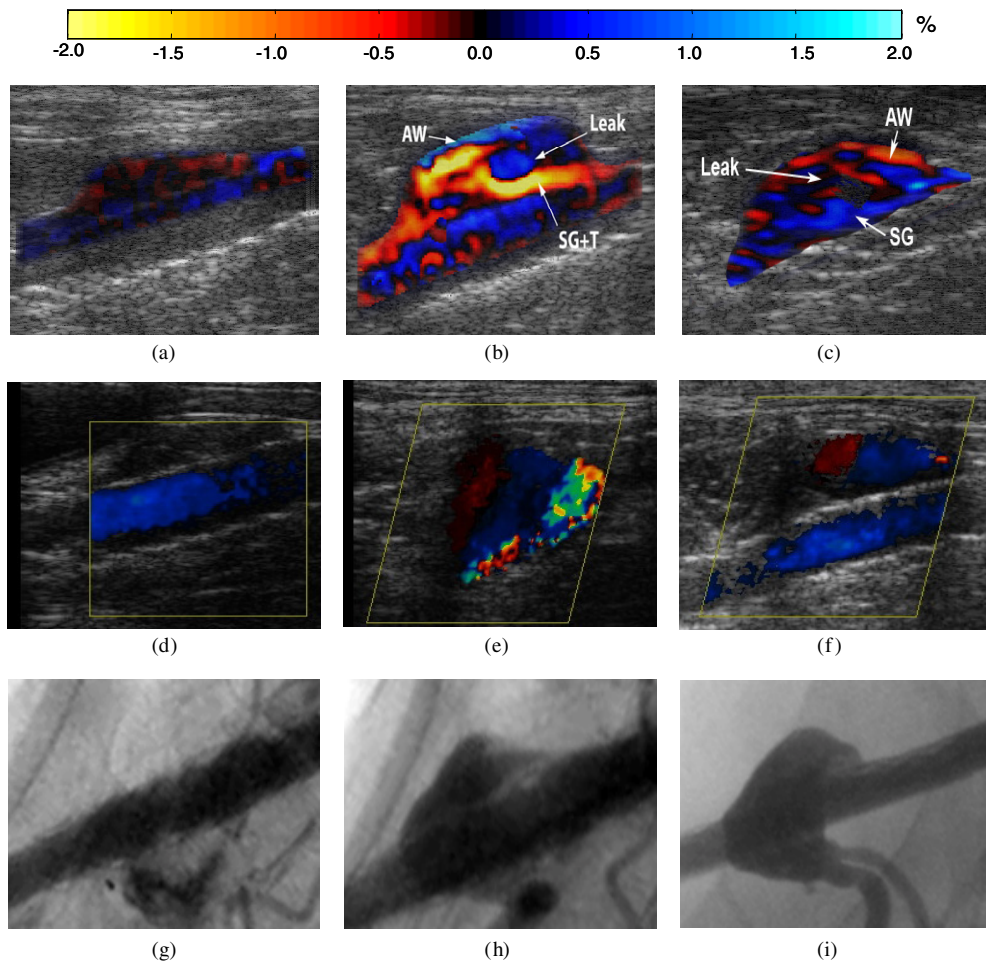
Figure 3. (a) Instantaneous elastogram, (d) color Doppler and (g) angiography of an aneurysm filled with a solid thrombus. No pulsation is observed in the sac, and strains (in black) are close to zero on the elastogram. (b) Instantaneous elastogram, (e) color Doppler and (h) angiography of an aneurysm with a partially thrombosed filled sac. On the elastogram the SG and solid thrombus appear in orange (SG + T) with a strain close to -1.5%, the artery wall (AW) and leak are in dark blue (strains are about 0.5%). Strain in the wall and strain in the solid thrombus have opposite signs, which is due to displacements in these two regions having opposite directions. (c) Instantaneous elastogram, (f) color Doppler and (i) angiography of an aneurismal sac with a large leak. On the elastogram, the SG appears in orange with a maximum strain close to -1.5%, the arterial wall (AW) is in blue with a strain of about 0.5%, and the leak corresponds to the fluctuating strain values within the sac. Arterial wall looks larger than its real size because surrounding tissues may deform equivalently.

tissues moved in opposite direction and were separated by the fluid blood. The blood likely experienced a lateral motion instead of a pure axial strain. This may have resulted in a wrong displacement within the calculation window causing a bad registration of the signals at the level of the thrombus, thus producing this opposite sign. Finally, the elastogram in figure 3(c) is characterized by the presence of color fluctuations of small magnitudes within the sac, the SG and arterial wall appearing again as homogeneous strain regions with opposite directions. This image represents an elastogram of a large leak. On these three images, the arterial wall

Table 2. Classification agreement between elastography and reference imaging (combination of color Doppler and angiography) to identify endoleaks following stent-graft implantation.

		Elastography classification			
		Leak > 50%	Leak < 50%	No leak	Total
Reference imaging classification	Leak > 50%	13	2	0	15
	Leak < 50%	2	8	0	10
	No leak	0	2	7	9
Total		15	12	7	34

likely looks larger than its real size because the strain map could include surrounding tissues deforming similarly as the vessel wall.

The classification agreement of endoleaks between elastography and combined color Doppler and angiography methods (reference imaging) is presented in table 2. A Kappa coefficient of 0.79 was obtained. Several tables exist for interpreting κ values (Sim and Wright 2005) but none is a universal standard, however for each of them a coefficient of 0.79 indicates a good agreement between two approaches. For comparison, the Kappa test between color Doppler and angiography was 0.84. This shows that no imaging methods could alone provide a faultless diagnosis of endoleaks. Among the 34 cases, there were 28 agreements between elastography and reference imaging. All leaks detected by combining color Doppler with angiography were also detected with elastography. Four cases of disagreement (4 out of 6) were close to the 50% threshold, but were classified in different categories.

Figure 4 presents the correlation between the percentage of solid thrombi estimated with elastography and with macroscopic sections. A correlation coefficient of 0.88 ($p < 0.001$) and a zero intercept ($y = x$) were obtained. This result should however be taken carefully, as the seven cases with 100% of thrombus entered in the calculation, the correlation was emphasized. A complementary information available with elastography is the pressurization of the sac by endoleaks potentially causing vessel wall cyclic pulsations. Such an analysis is presented in figure 5 where cumulated strains were quantified in the venous patch of the sac. As identified, no deformations were measured in a thrombosed sac (no leak), whereas strain pulsations within the venous patch were produced by a leak. From the entire database, cumulated strains of $0.06 \pm 0.06\%$ were measured in the absence of leak, compared with $2.24 \pm 1.12\%$ for large leaks ($p < 0.001$) and $2.16 \pm 1.17\%$ for small leaks ($p < 0.001$). The cumulated strain alone did not allow us to decide whether it was a small or a large leak ($p = 0.91$). To further assess the potential clinical impact of elastography, cumulated strain amplitudes within the venous patch from peak systole to end diastole were compared with the diameter expansion of the aneurysm measured in B-mode US. As seen in figure 6, a poor correlation ($r = 0.12$, $p = 0.5$) was obtained. Aneurysm expansion is a well-known criterion to evaluate the clinical importance of a leak. As reported in figure 5, elastography could detect the pressurization of the aneurismal sac but this measure does not appear to be sensitive to diameter changes over a three month period.

4. Discussion

4.1. Aneurysms without SG implantation

Table 1 showed that estimated strains were two times smaller in the venous patch than in the arterial wall (average values of $3.0 \pm 0.7\%$ versus $6.1 \pm 1.5\%$). High standard deviations could
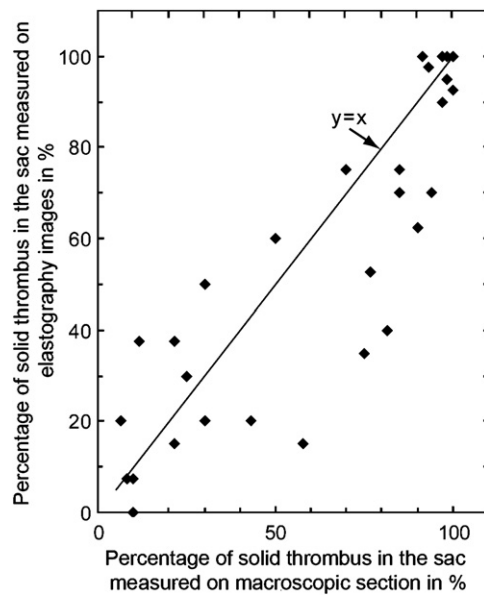
Figure 4. Correlation between percentage of solid thrombus in the sac measured on elastography images and on macroscopic sections.
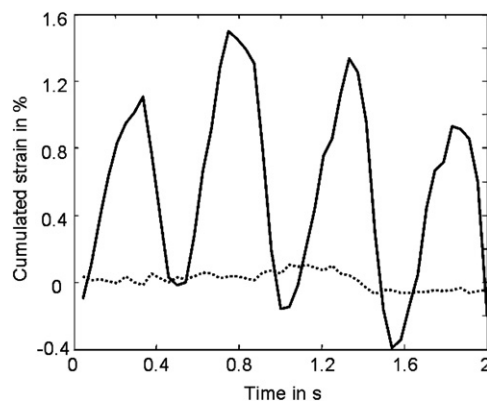
Figure 5. Cumulated strain profiles over four consecutive cardiac cycles measured on the aneurismal wall, for an aneurysm with a leak (plain line) and a thrombosed aneurysm without any leak (dotted line).

also be noted for the strain estimation, this is mainly due to the fact that each strain estimate was calculated from two different acquisitions (one cross sectional and one longitudinal). Attention was paid during acquisitions to place the probe to identify in-plane motion of the arterial wall, but changes in position and orientation of the probe between acquisitions increased the strain variance.

The elasticity ratios estimated in the current study are in the same order of magnitude as other studies comparing mechanical properties of arteries and veins (Wesly *et al* 1975, Baird and Abbott 1977, Salacinski *et al* 2001). For example, Baird and Abbott (1977) reported in
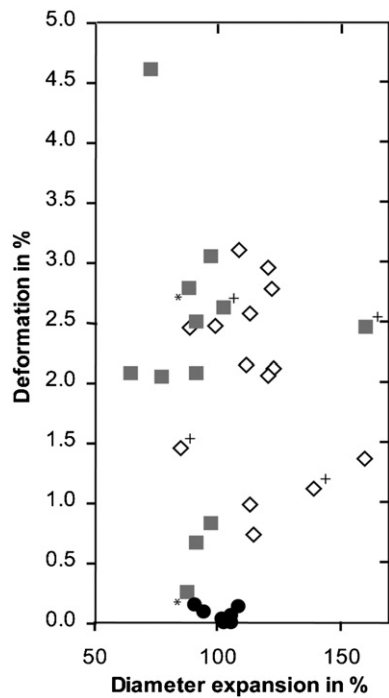
Figure 6. Cumulated strain within the venous patch between peak systole and end diastole as a function of the aneurysm diameter expansion measured in B-mode ultrasound three months after SG implantation. The symbol ◇ represents large leaks, ■ are small leaks and ● corresponds to the absence of leak, as detected by elastography. The symbol + indicates four leaks classified at different sizes by the reference imaging methods (angiography and color Doppler) and ∗ indicates the two cases detected without leak on reference imaging.

a canine model that the jugular vein was less compliant than the carotid artery. Veins also had a higher incremental stress modulus than arteries. The incremental stress modulus is the ratio of changes in wall stress to changes in arc length. For pressures varying from 80 to 160 mmHg, stress modulus ratios between jugular veins and carotid arteries varied from 7.8 to 5.1. Note that none of previous studies (Wesly *et al* 1975, Baird and Abbott 1977, Salacinski *et al* 2001) estimated a similar elasticity parameter, so it is not obvious to compare our results on cumulated strains. As also noted in table 1, cumulated strains varied between dogs ($p < 0.02$), possibly due to differences in systemic pressures between animals and changes in probe position between acquisitions. When normalizing the impact of pressure differences by computing the ratio of cumulated strains in the venous patch to that in the arterial wall for each dog, statistical similarity was then observed between animals ($p = 0.68$).

4.2. Aneurysms after EVAR

This study confirmed that advantages of elastography are to provide images of the solid thrombus expanse (figure 4) and that of endoleaks when present (figures 2 and 3). We also showed in figure 5 that vessel wall cyclic deformations within the aneurismal sac could confirm the presence of endoleaks. In addition, we reported a good agreement between elastography and reference imaging methods ($\kappa = 0.79$) for endoleak characterization. Note, however,

that elastograms were post-processed offline contrary to angiography and color Doppler US that were acquired with live optimization of image quality. This is an important difference in favor of the reference imaging modalities because the acquisition of RF data, used to compute elastograms, was based on B-mode image feedback with no information on tissue elasticity. Some elastograms were globally decorrelated over the whole image plane and were then difficult to interpret when post-processed, especially in the systolic phase where motion between successive RF images is more important. Twelve RF sequences among the 136 acquired in this study could not be used because of the poor image quality (low SNR, high global motion). Nevertheless, by combining the diagnostic information from the four longitudinal and cross-sectional sections acquired for each aneurysm allowed us to reduce the risk of misinterpretation. A real-time implementation of our elastography algorithm on a clinical scanner would certainly improve the quality of the diagnosis because of the image acquisition biofeedback. Note that the clinical gold standard imaging modality for aneurysm follow-up is CT scan but this modality was not available in this study.

By definition, a successful EVAR with a good seal should lead to low sac pressurization and a loss of pulsatility (Sonesson *et al* 2003). Several studies showed, during and 24 hours after SG implantation, that the absence of leak gives a lack of pulsation (Treharne *et al* 1999, Gawenda *et al* 2002). Baum *et al* (2001) observed systemic sac pressurization after 30 days post EVAR, in the presence of endoleaks (type I or type II). However, opinion differs about the loss of pulsatility in healed aneurysms, and researchers think that pressure may be transmitted directly through the SG fabric (Wilson *et al* 2001). Thus, monitoring of pulse pressure related deformations of vascular wall within aneurismal sac is of clinical relevance. With elastography that can monitor the thrombus size, importance of leaks and vessel wall cyclic deformations due to sac pressurization, controversies as to whether SG fabric may transmit pulsatility within a healed aneurysm may be solved. In our study, no periodic strain was observed in any of the seven aneurysms diagnosed healed with both elastography and the reference imaging method (table 2). However, for the two false positives, periodic strains were observed. For one of these two misclassifications, periodic strains within the venous patch were observed but motion periodicity was not synchronized with the cardiac frequency, which may suggest respiratory or operator artifact movements. For the other misclassification, the aneurismal sac was completely filled with a solid thrombus but the collateral vessel was still patent and could have induced sac pressurization through the thrombus (not detected with color Doppler and angiography but present on macroscopic analysis).

Current results tend to show that elastography is a good modality to provide additional information preoperatively on mechanical properties of aneurysms as well as for their follow-up after EVAR. CT scan is the most efficient tool to characterize and follow AAA after EVAR (AbuRahma *et al* 2005) but it exposes patients to the hazard of contrast injection and irradiation and the cost of a CT exam is much higher than that of ultrasound. Moreover, CT cannot estimate mechanical properties of aneurysm components. Elastography, as color Doppler, does not possess CT accuracy but it has the advantage of being noninvasive. Compared to other US-based imaging approaches such as color Doppler that measures flow velocity and M-mode pulsatile wall motion estimation, elastography has the advantage to provide a 2D image of thrombus deformation within the sac, which are not visible on B-mode images. In the present study, a relatively high frequency probe was used to image aneurysms, taking advantage that dog iliac arteries are close to the skin. However, it could be a problem for AAA in humans, where a lower frequency probe is required thus decreasing the spatial resolution of images.

In conclusion, US elastography is a good complementary tool to B-scan and color Doppler to characterize aneurysms following EVAR. This technique detected all leaks and allowed

differentiation within the aneurismal sac of solid thrombi, presence of leak areas and pulsatile deformations of the venous patch of the proposed dog model. The noninvasive elastography method was in very good agreement with the reference combined imaging modality to estimate the thrombosed portion of the aneurysm and it might help during the follow-up to detect complications after EVAR. A 3D visualization may provide a better estimation of the solid thrombus expanse in the sac; this can be a potential avenue of development. Quantitative results before SG implantation provided consistent information on mechanical properties of normal arterial walls and venous patches, and on sac pulsatility.

Acknowledgments

References

AbuRahma A F, Welch C A, Mullins B B and Dyer B 2005 Computed tomography versus color duplex ultrasound for surveillance of abdominal aortic stent-grafts *J. Endovasc. Ther* **12** 568–73

Baird R N and Abbott W M 1977 Elasticity and compliance of canine femoral and jugular vein segments *Am. J. Physiol.* **233** H15–H21

Baum R A, Carpenter J P, Cope C, Golden M A, Velazquez O C, Neschis D G, Mitchell M E, Barker C F and Fairman R M 2001 Aneurysm sac pressure measurements after endovascular repair of abdominal aortic aneurysms *J. Vasc. Surg.* **33** 32–41

Brusseau E, Fromageau J, Finet G, Delachartre P and Vray D 2001 Axial strain imaging of intravascular data: results on polyvinyl alcohol cryogel phantoms and carotid artery *Ultrasound Med. Biol.* **27** 1631–42

Cespedes I, Ophir J, Ponnekanti H and Maklad N 1993a Elastography: elasticity imaging using ultrasound with application to muscle and breast *in vivo Ultrason. Imaging* **15** 73–88

Cespedes I and Ophir J 1993b Reduction of image noise in elastography *Ultrason. Imaging* **15** 89–102

Chaer R A, Trocciola S, DeRubertis B, Hynecek R, Xu Q, Lam R, Kent K C and Faries P L 2006 Evaluation of the accuracy of a wireless pressure sensor in a canine model of retrograde-collateral (type II) endoleak and correlation with histologic analysis *J. Vasc. Surg* **44** 1306–13

de Korte C L, van der Steen A F, Céspedes E I and Pasterkamp G 1998 Intravascular ultrasound elastography in human arteries: initial experience *in vitro Ultrasound Med. Biol.* **24** 401–8

EVAR Trial Participants 2005 Endovascular aneurysm repair versus open repair in patients with abdominal aortic aneurysm (EVAR trial 1): randomized controlled trial *Lancet* **365** 2179–86

Gawenda M, Heckenkamp J, Zaehringer M and Brunkwall J 2002 Intra-aneurysm sac pressure–the holy grail of endoluminal grafting of AAA *Eur. J. Vasc. Endovasc. Surg.* **24** 139–45

Gorham T J, Taylor J and Raptis S 2004 Endovascular treatment of abdominal aortic aneurysm *Br. J. Surg.* **91** 815–27

Greenhalgh R M 2004 Comparison of endovascular aneurysm repair with open repair in patients with abdominal aortic aneurysm (EVAR trial 1), 30-day operative mortality results: randomised controlled trial *Lancet* **364** 843–8

Hinnen J W, Koning O H, Vlaanderen E, van Bockel J H and Hamming J F 2006 Aneurysm sac pressure monitoring: effect of pulsatile motion of the pressure sensor on the interpretation of measurements *J. Endovasc. Ther.* **13** 145–51

Hinnen J W, Rixen D J, Koning O H, Van Bockel H J and Hamming J F 2007 Aneurysm sac pressure monitoring: does the direction of pressure measurement matter in fibrinous thrombus? *J. Vasc. Surg* **45** 812–6

Hiramoto J S, Reilly L M, Schneider D B, Sivamurthy N, Rapp J H and Chuter T A M 2007 Long-term outcome and reintervention after endovascular abdominal aortic aneurysm repair using the Zenith stent graft *J. Vasc. Surg.* **45** 461–6

Hoyert D L, Heron M P, Murphy S L and Kung H-C 2006 Deaths: Final Data for 2003 *National Vital Statistics Reports* **54** 120

Konofagou E E, Varghese T, Ophir J and Alam S K 1999 Power spectral strain estimators in elastography *Ultrasound Med. Biol.* **25** 1115–29

Lasheras J C 2007 The biomechanics of arterial aneurysms *Annu. Rev. Fluid Mech.* **39** 293–319

Lerouge S, Raymond J, Salazkin I, Qin Z, Gaboury L, Cloutier G, Oliva V L and Soulez G 2004 Endovascular aortic aneurysm repair with stent-grafts: Experimental models can reproduce endoleaks *J. Vasc. Interv. Radiol.* **15** 971–9

Maurice R L and Bertrand M 1999 Lagrangian speckle model and tissue-motion estimation—theory *IEEE Trans. Med. Imag.* **18** 593–603

Maurice R L, Brusseau E, Finet G and Cloutier G 2005a On the potential of the Lagrangian speckle model estimator to characterize atherosclerotic plaques in endovascular elastography: *in vitro* experiments using an excised human carotid artery *Ultrasound Med. Biol.* **31** 85–91

Maurice R L, Daronat M, Ohayon J, Stoyanova E, Foster F S and Cloutier G 2005b Non-invasive high-frequency vascular ultrasound elastography *Phys. Med. Biol.* **50** 1611–28

Nightingale K, Soo M S, Nightingale R and Trahey G 2002 Acoustic radiation force impulse imaging: In vivo demonstration of clinical feasibility *Ultrasound Med. Biol.* **28** 227–35

Ophir J, Cespedes I, Ponnekanti H, Yazdi Y and Li X 1991 Elastography—a quantitative method for imaging the elasticity of biological tissues *Ultrason. Imaging* **13** 111–34

Parker K J, Huang S R, Musulin R A and Lerner R M 1990 Tissue response to mechanical vibrations for 'sonoelasticity imaging' *Ultrasound Med. Biol* **16** 241–6

Pesavento A, Perrey C, Krueger M and Ermert H 1999 A time-efficient and accurate strain estimation concept for ultrasonic elastography using iterative phase zero estimation *IEEE Trans. Ultrason. Ferro. Freq. Control* **46** 1057–67

Prinssen M, Verhoeven E L, Buth J, Cuypers P W, van Sambeek M R, Balm R, Buskens E, Grobbee D E and Blankensteijn J D 2004 A randomized trial comparing conventional and endovascular repair of abdominal aortic aneurysms *N. Engl. J. Med* **351** 1607–18

Raymond J, Sauvageau E, Salazkin I, Ribourtout E, Gevry G and Desfaits A-C 2002 Role of the endothelial lining in persistence of residual lesions and growth of recurrences after endovascular treatment of experimental aneurysms *Stroke* **33** 850–5

Ribbers H, Lopata R G, Holewijn S, Pasterkamp G, Blankensteijn J D and de Korte C L 2007 Noninvasive two-dimensional strain imaging of arteries: validation in phantoms and preliminary experience in carotid arteries *in vivo Ultrasound Med. Biol.* **33** 530–40

Salacinski H J, Goldner S, Giudiceandrea A, Hamilton G, Seifalian A M, Edwards A and Carson R J 2001 The mechanical behavior of vascular grafts: a review *J. Biomater. Appl.* **15** 241–78

Sandrin L, Catheline S, Tanter M, Hennequin X and Fink M 1999 Time-resolved pulsed elastography with ultrafast ultrasonic imaging *Ultrason. Imaging* **21** 259–72

Schaar J A, de Korte C L, Mastik F, Strijder C, Pasterkamp G, Boersma E, Serruys P W and van der Steen A F W 2003 Characterizing vulnerable plaque features with intravascular elastography *Circulation* **108** 2636–41

Schmitt C, Soulez G, Maurice R L, Giroux M -F. and Cloutier G 2007 Non-invasive vascular elastography: toward a complementary characterization tool of atherosclerosis in carotid arteries *Ultrasound Med. Biol.* **33** 1841–58

Schurink G W, Aarts N J, Malina M and van Bockel J H 2000 Pulsatile wall motion and blood pressure in aneurysms with open and thrombosed endoleaks—comparison of a wall track system and M-mode ultrasound scanning: an in vitro and animal study *J. Vasc. Surg.* **32** 795–803

Seriki D M, Ashleigh R J, Butterfield J S, England A, McCollum C N, Akhtar N and Welch C 2006 Midterm follow-up of a single-center experience of endovascular repair of abdominal aortic aneurysms with use of the Talent stent-graft *J. Vasc. Interv. Radiol.* **17** 973–7

Sim J. and Wright C. C. 2005 The Kappa statistic in reliability studies: use, interpretation, and sample size requirements *Phys. Ther.* **85** 257–68

Sonesson B, Dias N, Malina M, Olofsson P, Griffin D, Lindblad B and Ivancev K 2003 Intra-aneurysm pressure measurements in successfully excluded abdominal aortic aneurysm after endovascular repair *J. Vasc. Surg.* **37** 733–8

Soulez G, Lerouge S, Salazkin I, Darsaut T, Oliva V L and Raymond J 2007 Type I and collateral flow in experimental aneurysm models treated with stent-grafts *J. Vasc. Interv. Radiol.* **18** 265–72

Sun Z 2006 Diagnostic value of color duplex ultrasonography in the follow-up of endovascular repair of abdominal aortic aneurysm *J. Vasc. Interv. Radiol* **17** 759–64

Thomas S M, Beard J D, Ireland M and Ayers S 2005 Results from the prospective registry of endovascular treatment of abdominal aortic aneurysms (reta): mid term results to five years *Eur. J. Vasc. Endovasc. Surg.* **29** 563–70

Treharne G D, Loftus I M, Thompson M M, Lennard N, Smith J, Fishwick G and Bell P R 1999 Quality control during endovascular aneurysm repair: monitoring aneurysmal sac pressure and superficial femoral artery flow velocity *J. Endovasc. Surg.* **6** 239–45

Uflacker R and Robison J 2001 Endovascular treatment of abdominal aortic aneurysms: a review *Eur. Radiol* **11** 739–53

Veith F J *et al* 2002 Nature and significance of endoleaks and endotension: summary of opinions expressed at an international conference *J. Vasc. Surg* **35** 1029–35

Wesly R L, Vaishnav R N, Fuchs J C, Patel D J and Greenfield J C 1975 Static linear and nonlinear elastic properties of normal and arterialized venous tissue in dog and man *Circ. Res* **37** 509–20

Wilson K A, Lindholt J S, Hoskins P R, Heickendorff L, Vammen S and Bradbury A W 2001 The relationship between abdominal aortic aneurysm distensibility and serum markers of elastin and collagen metabolism *Eur. J. Vasc. Endovasc. Surg.* **21** 175–8